Development of an ultrafast, time-resolved Schlieren imaging system

A thesis submitted in partial fulfillment of the requirement
for the degree of Bachelors of Science in Physics from
The College of William and Mary

by

Justin Deighan

Accepted for _____
(Honors)

_____
Gina L. Hoatson

_____
Eugene R. Tracy

_____
Gunther Luepke

_____
Jan Chaloupka

Williamsburg, VA
May 2007

Abstract

An iterative technique has been developed by which reproducible high speed phenomenon such as laser filamentation and electrical discharges may be imaged at high temporal and spatial resolution. By continuously repeating a triggerable event and taking an ultrafast still Schlieren image at a set time in relation to the trigger, a steady stream of frames of similar events at the same step of evolution is generated. If the event is repeated at a rate over the flicker fusion threshold the stream of frames will appear as a steady image to an observer, representing the average state of an event at a set point in its evolution. By adjusting the time difference between the event trigger and image generation, the observed point in time can be arbitrarily chosen. The temporal resolution of this Real-Time Iterative Sampling (RTIS) method is limited by the time difference jitter and can easily be in the subnanosecond region using semiconductor based triggering. This provides access to time regimes previously inaccessible to CCD cameras while maintaining still image quality impossible to obtain by streak camera methods.

Acknowledgments

I would like to express my gratitude to Dr. Chaloupka for his ideas and guidance, Thomas Ruscher for his tools and advice, Sara Hanners for her support and assistance, and Joshua Street for just being there.

Contents

1 Introduction

The use of high-speed imaging is an invaluable tool in the study of a wide range of phenomena on the current frontiers of science. Applications range from laser filamentation and electrical discharges and the interactions between them [1-11] to such fields as ultrasonics [12], sonoluminescence [13], and laser ablation [14]. While a single still frame of a high-speed event can be very informative, a method detailing the temporal evolution of the event is more desirable. The two most advanced techniques in use today are CCD cameras, which produce a sequence of still images, and streak cameras, which produce a single image with one of the two spatial axes sacrificed to become a temporal axis. These methods are often paired with a Schlieren system to image the refractive index gradient of the transparent medium in which the phenomenon occurs (air, water, oil, etc.), providing deeper insight into the underlying mechanisms [6,7,9,12]. The usefulness of these two methods in studying high-speed phenomena are limited primarily by their temporal resolution. Currently, the cutting-edge of CCD camera technology is capable of 100 million frames per second [15], equivalent to a temporal resolution of 10 ns, while photoelectric streak camera techniques have been capable of resolutions under 100 ps for over a decade [16]. However, the informational value of the streak camera image is inferior to a CCD sequence of equal temporal resolution because it can record only a single spatial dimension.

An alternative high-speed imaging solution for reproducible events that retains the CCD camera's 2D still frame qualities while achieving a subnanosecond temporal

resolution is set forth here. This Real-Time Iterative Sampling (RTIS) technique operates by generating a continuous train of triggered events along with a synchronized pulsed Schlieren system and CCD camera. The imaging system is set to generate a still image at a specified time in relation to the trigger, producing a stream of frames of similar events at the same stage of evolution. As the frequency of the event train is increased, the impression of an observer viewing the image train transitions from that of a flickering sequence of stills to that of a constant image. At this point, usually around 50Hz, the frequency has passed the so-called flicker fusion rate and the stream of frames will appear to an observer as a steady image of an averaged event at a certain point in its temporal evolution [17]. The temporal location of the observed point may be arbitrarily chosen in real-time by adjusting the time difference between the event trigger and image generation. It is the jitter in this time difference that defines the ultimate temporal resolution. Candidate phenomena for this technique require good reproducibility and the ability of the environment to fully relax between events.

To demonstrate the capabilities of this technique a semiconductor triggered inductive spark gap and ultrafast laser Schlieren imaging system have been designed, built, and tested. Using off-the-shelf semiconductor based triggering and delay equipment, triggering jitter below 100 picoseconds was achieved. Due to the limitations of the spark coil and Schlieren system used, generation of an RTIS image with spatial resolution capable of discerning spark gap breakdown was not achieved. However, combining evidence from previous studies with the results presented here confirm the validity of the experiment's basic concept as a proof-of-principle for the RTIS technique.

2 Background and Theory

2.1 The Schlieren Method

In order to observe the effects of an electrical arc discharge in air an imaging technique capable of discerning thermal and density gradients with ultrashort exposure time was required for the study. The basis for the method that was decided upon was the venerable Schlieren system, with the modifications of using an ultrashort pulsed Ti:Sapphire laser beam as the light source and capturing the final image on a CCD camera.

The Schlieren optical effect was first observed with candle light sources by Robert Hooke in 1665 and the modern Schlieren system was designed by August Toepler in the early 19th century to detect aberrations in glass optical lenses [18]. It was Toepler who named the Schlieren method after the German word for "streak", a reference to the twisted images of flowing medium that the technique produces. A modified version of the Schlieren system was developed by Oppenheim et. al. in 1965 using the newly invented visible laser instead of a conventional white arc lamp [19]. This design allowed exposure times on the nanosecond scale and provided a light source bright enough to outshine, and thus image, such subjects as electrical arcs and plasma jets. The full capabilities of this method were relevantly exemplified by Thomas in 1973 when he successfully obtained image sequences of dielectric breakdown in liquids using an ultrafast laser Schlieren technique [7].

The flexibility and power demonstrated by the Schlieren system over the past few

centuries is remarkable considering the subtlety and simplicity of the mechanism by which it operates. It is well known that when a beam of light passes through a transparent medium it will deflect slightly in response to any gradient of the refractive index. A common example of this is the refraction that occurs at the interface between two media with differing refractive index, such as air and water at the surface of a pool or in a glass. The same effect occurs with much lower deflection within a single medium when light passes through a density gradient caused by thermal or physical shock. In a gas the relationship between the refractive index and density is given by the Gladstone-Dale formula:

$$n = 1 + k\rho \tag{1}$$

where n is the refractive index, k is the Gladstone-Dale coefficient characteristic of the gas and light wavelength, and ρ is the gas density. The possible ways in which the density of a gas might be modified are succinctly described through a manipulation of the ideal gas law:

$$\rho = \frac{p}{RT} \tag{2}$$

where T is the gas temperature, R the specific gas constant, and p the pressure. Thus we find that thermal and pressure gradients may produce deflections in light rays. The thermal effect can occasionally be observed on an especially hot or cold day and is commonly referred to as a mirage [20]. However, this effect is extremely slight. This is because the factor $k\rho$ in Eq. 1 is typically very small, being only about 0.000292 for air at STP in the visible spectrum, which makes the value of n very close to unity [21]. This explains why density gradients are not usually perceptible in daily life. Even if the

density of a region of air was increased by 100 times its standard value, the refractive index would change by barely 3%. And yet, it is this nearly imperceptible refraction of light caused by density gradients that is the basis of the Schlieren effect.

In the basic Schlieren system the light from a point source is expanded through a lens and collimated into a wide beam. This beam is passed through a volume of transparent medium containing the event to be imaged and then focused down to a point before re-expanding onto a viewing screen or camera. As the collimated beam interacts with density gradients in the imaging volume the light is deflected slightly off its original straight course. In order to highlight these deflections a sharp straight knife edge is added at the focal point of the beam after the imaging volume. Based on the nature of the gradients encountered in the imaging volume, portions of the beam's image will be shifted slightly toward or away from the knife edge, those that strike the blade being removed from the final image while those missing it being allowed to continue on. This causes the intensity of the final image to be modified in proportion to the density gradient normal to the knife edge in the volume. Any ray displacement parallel to the knife edge, however, will have no effect on the final image. A diagram of a Z-type Schlieren system following the described method is depicted in Fig. 1.

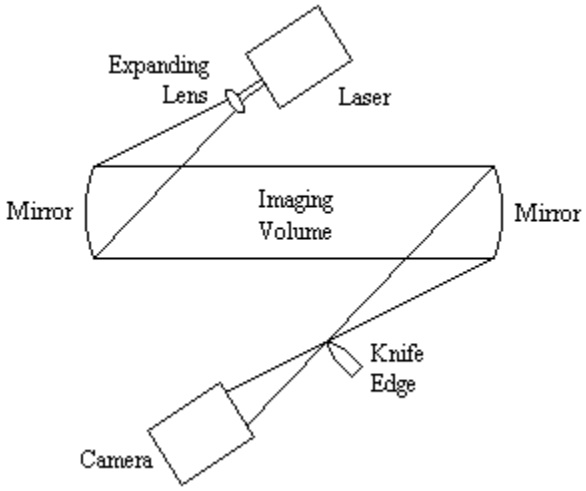

Fig. 1: A typical Z-type laser Schlieren system, named for its characteristic 'Z' shaped light path. Schlieren produced by refractive index gradients in the imaging volume are highlighted by the knife edge at the focal point and imaged by the camera.

To quantitatively describe a light ray's differential angle of refraction $d\varepsilon$ caused by traveling a distance dx through a gradient dn/dy we align a coordinate system such that the x-axis is parallel to the direction of light propagation and the y-axis is parallel to the gradient. We may then describe $d\varepsilon$ as (see App. A for the derivation):

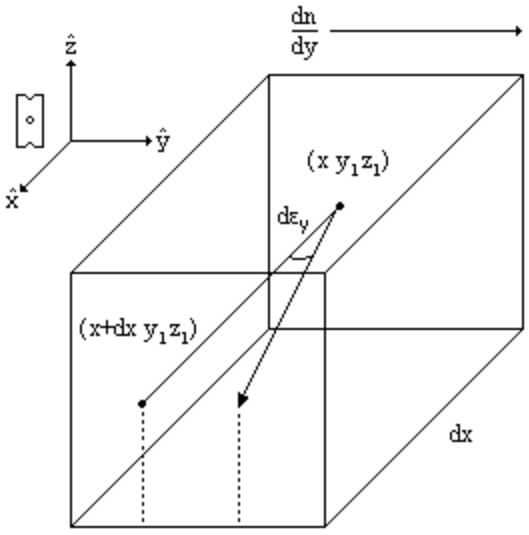

Fig. 2: Differential refraction of light through an angle $d\varepsilon_y$ over a distance dx caused by a refractive index gradient dn/dy.

$$d\varepsilon_y = \frac{1}{n}\frac{\partial n}{\partial y}dx \qquad (3)$$

where n is the refractive index as a function of position (x, y, z). A geometrical representation of the system is depicted in Fig. 2. The orientation of the system with respect to the knife edge is shown by a razor blade next to the coordinate vectors. In order to find the total deflection over an imaging volume of length L, such as in Fig. 1, we simply integrate to obtain:

$$\varepsilon_y = \int_o^L \frac{1}{n}\frac{\partial n}{\partial y}dx \qquad (4)$$

When the deflected light rays are focused down at the knife edge their image will be offset from the position of an undisturbed image by a distance:

$$\Delta a = f\tan(\varepsilon_y) \approx f\cdot\varepsilon_y \qquad (5)$$

where f is the focal length of the second mirror in Fig. 1. The contrast of the final image is determined by the fractional increase in intensity of the light passing the knife because of the deflected rays and may be expressed as:

$$C = \frac{\Delta I}{I} = \frac{\Delta a}{a} = \frac{f}{a}\varepsilon_y \tag{6}$$

where a is the distance the undisturbed image projects from the knife edge (see Fig. 3). From this equation we see that optimum contrast can be achieved in the Schlieren image by maximizing the focal length of the mirrors used, maximizing the angle ε, and by making the projecting area of the undisturbed area as small as possible. Focal length is of course limited by the space available for the Schlieren apparatus. It turns out that raising the wavelength of the light source increases the Gladstone-Dale coefficient in Eq. 1 and thus increases the refraction angle ε [21]. Simply blocking most of the focal point light with the knife to minimize the distance a makes the final image very dim. A better way of reducing a is to utilize low aberration parabolic mirrors and an imaging light source as point like as possible to decrease the total image size at the focal point.

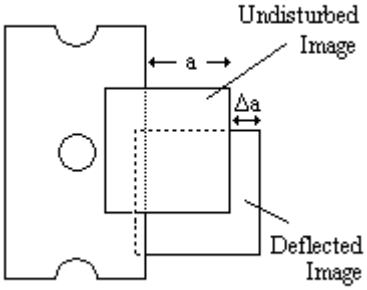

Fig. 3: Cross-section of undisturbed and gradient deflected focal images at the knife edge in a Schlieren system.

2.2 Triggered Spark RTIS Candidacy and Objectives

Not all phenomenon may be usefully imaged using the RTIS technique. Events which cannot be reliably reproduced or from which the environment cannot completely (or nearly completely) relax in less than a tenth of a second will not give interesting results as the image will experience excessive spatiotemporal blur. In this section the

general applicability of the RTIS technique and (more specifically) its appropriateness for imaging semiconductor triggered sparks in a tabletop setting are explored, along with the design objectives for such an experiment.

Reproducibility for RTIS in General

While reproducibility is an essential requirement for any scientific experiment, it is especially important in RTIS based imaging. Here precise event reproducibility in both time and space is required. As the range of individual images' deviations increase the spatiotemporal resolution of the composite average suffers. Consider the composite averaged event as describing a finite line of connected points in time and space. Purely spatial blur occurs when, for a given sampled event within the composite, a given point in the series deviates from the average line in space but occurs at the average time after the trigger. Purely temporal blur occurs when a given point deviates from the average line in time but is identical

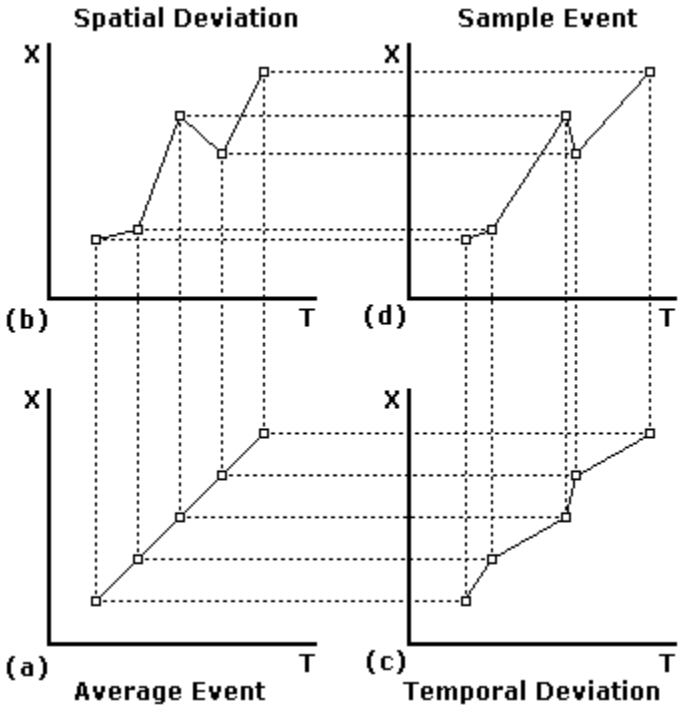

Fig. 4: Examples of types of spatiotemporal deviation from an average event (a), showing purely spatial (b), purely temporal (c), and spatiotemporally coupled (d) deviations.

to the average in spatial position. More often than not, however, both occur simultaneously, see Fig. 4, and the two may even be coupled via a physical relation.

Two types of spatio-temporal deviation may exist for a given event: original and rate. Original deviation, otherwise known as jitter, occurs when an event is triggered at a location in time or space that is different from that of the average origin. It arises primarily from inaccuracies in the event's triggering method. Rate deviation is a much more complex factor and takes into account all elements of the environment that alter the evolution of an event. It depends primarily upon the nature of the phenomenon being imaged.

The relative con-tributions of original and rate deviation to the total deviation of a sample event can vary dramatically among phenomena. As a spatial example, a coronal electric discharge from a point electrode may have a constant origin but wildly variable evolution, while a sonoluminescent bubble may have a very well defined evolution but be difficult to repeatedly trigger in exactly the same location. The deviation in the later case was cleverly eliminated by Pecha et. al. when computationally averaging together many streak camera images of bubble evolution by aligning all the samples based on their centers of gravity [13]. In this way they were able produce a more accurate integrated average of a sonoluminescent bubble's evolution and obtain better statistics. While not addressed in detail here, it is possible that this computational spatial jitter correction might be applied to RTIS for more accurate resolution. A calculation such as identifying a bubble in an image, locating its center of mass, and realigning the image in real-time synchronization with the image train is quite possible with modern computer technology.

Triggered Spark Reproducibility

The objective of synchronizing a triggered spark gap with an ultrafast imaging laser pulse at sufficiently low deviation to enable useful temporal resolution seemed somewhat daunting at first. Moreover, while original spatial jitter may be negligible for point electrodes, significant systematic jitter would be introduced by the finiteness of the illuminating pulse's exposure time if it was not short enough. In order to assess the possibility of achieving these goals it was necessary to produce an estimate of the timescale on which dielectric breakdown in a gas operates. A rough calculation may be performed by finding the transit time for an electron in a dielectric gas between two conductive parallel plates inside which there exists an electric field equal to the dielectric breakdown point of the gas. The time for an electron to cross the gap between the plates is:

$$t = \frac{d}{v_d} \tag{7}$$

where v is the velocity of the electron in the gas and d is the distance between the electrodes. For air at STP in a breakdown electric field of ~30 kV/cm [22] an electron drift velocity of ~1.4×10^5 m/s is interpolated from the compiled values of Roznerski and Leja [23]. This compares well with the $1x10^5$ m/s found for a lightning leader stroke by Wurden and Whiteson [10]. Such a measurement was possible due to the great distance covered by a lightning bolt, on the order of kilometers, causing breakdown timescales to be on the order of tens of milliseconds. At such speeds there are no obstacles to CCD still

sequences.

While a velocity of $1x10^5$ m/s is a good estimate for the infinite plane approximation in air, non-planar geometries may produce much larger speeds. Using a point to plane geometry Allen and Ghaffar [4] observed a positive streamer velocity on the order of $0.1\text{-}1\times10^6$ m/s for corona discharges in air, which is supported by the values found by Veldhuizen and Rutgers [5]. These values for a gas may be contrasted with the much lower velocities found in dielectric liquids. Both Massala and Lesaint [8] and Nakao et. al. [9] found point to plane positive streamer velocities on the order of 1×10^3 m/s for mineral transformer oil and liquid alkanes respectively. Both used a minimum electrode gap on the order of 1 cm, implying a breakdown timescale of 10 μs according to Eq. 7. In this regime Massala and Lesaint were able to produce streak camera images with very good temporal resolution and Nakao et. al. used a 1 million fps CCD camera to generate useful sequences of images.

When considering similar experiments in air, however, the greater velocity of the breakdown drives the timescale down to tens of nanoseconds, which is just beyond the reach of cutting-edge CCD technology [15]. In order to obtain useful sequences of images of such events temporal resolution must be on the nanosecond scale or faster. In addition, to secure still frames with less than 1% systematic spatial jitter requires exposure times bordering on the picosecond regime. This imposed a subnanosecond temporal jitter constraint for the triggered spark generator design and picosecond or faster pulse length for the laser.

In order to design a spark trigger for minimal temporal jitter some understanding

of semiconductor switching is necessary. In a digital switch there are two basic factors that determine signal jitter: voltage deviation and slew rate. An illustration of this relation is depicted in Fig. 5. The falling edge of two pulses with slew rate S are shown falling from two voltages with difference ΔV. If both edges begin falling at the same time, their drop to some value V' will be offset by a time Δt. This time differential may be expressed as:

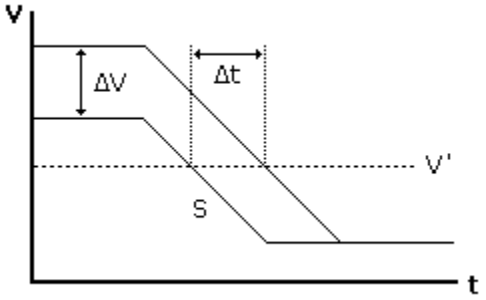

Fig. 5: A geometric representation of the temporal jitter Δt caused by a voltage instability ΔV in a falling edge of slope S.

$$\Delta t = \frac{\Delta V}{S} \tag{8}$$

When this difference is used to describe the temporal deviation of the falling edge from its intended position it describes the temporal jitter. It is apparent from Eq. 8 that this jitter may be minimized by reducing ripple and noise in the circuit's reference voltage and selecting a high-speed switch with a large slew rate.

While original spatiotemporal jitter may be minimized by design, rate deviation is not as directly under the experimentalist's control. However, given an unobstructed 1 cm spark gap between point electrodes or a point-plane geometry, the arc will follow a relatively straight path and spatial deviations can be assumed to be less than 1 mm. This is a small enough spatial resolution that it should reveal evolution across the spark gap. According to Eq. 7 this corresponds to a temporal resolution of less than 1 nanosecond at a breakdown velocity of 1×10^6 m/s, which lies within the range of acceptable temporal deviation determined above.

Relaxation for RTIS in General

The second requirement for RTIS candidate phenomenon is the ability of the surrounding environment to relax back to a state similar to the initial one before the next event in the train. If the environment is not allowed to fully relax between events then the individual samples will not be representative of an isolated event and the averaged image will be skewed. Let us take as a relevant example the relaxation of dielectric strength in an insulating fluid that has been subjected to dielectric breakdown. Fig. 6(a) shows a totally isolated breakdown event and the environment's subsequent relaxation to full dielectric strength over a time period t_R. If a train of events is triggered at a rate with a period greater than t_R, as in Fig. 6(b), each individual event is sufficiently isolated that images of each taken a fixed delay after the trigger (but before the next) will be representative of a completely isolated event. However, if the train of events is triggered at a rate with a

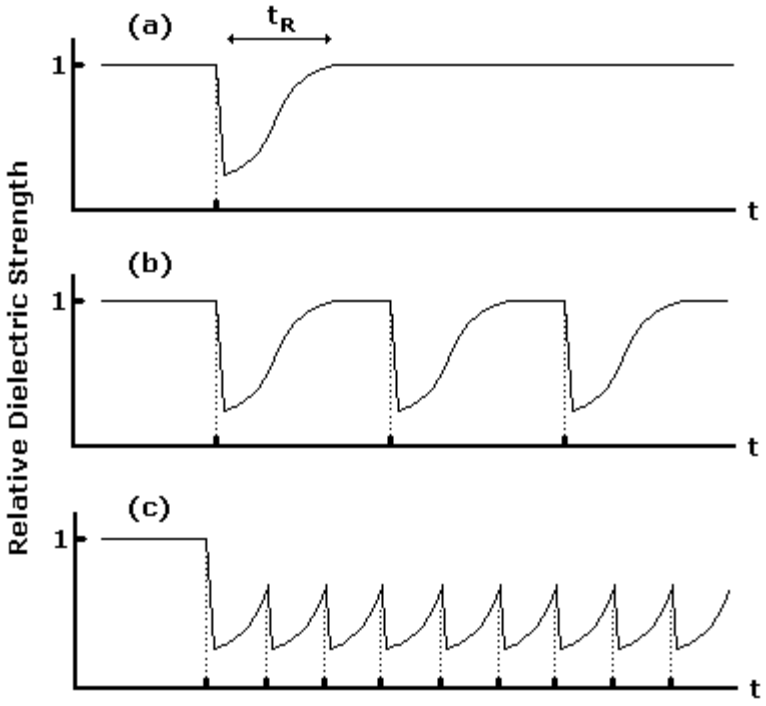

Fig. 6: Dielectric breakdown example of relaxation. (a) A single breakdown is triggered and the environment relaxes after a time t_R, (b) a train of breakdowns with a rep-rate period greater than t_R, (c) a train of discharges is triggered at a rep-rate period less than t_R.

period shorter than t_R, as in Fig. 6(c), the environment does not have time to fully relax and each iteration is no longer representative of an isolated event. Instead, the temporal relaxation characteristics are cut short and a systematic steady-state effect is introduced, in this case a lowering of the maximum dielectric strength that the system is allowed to relax to after each event. While the imaging of events with such truncated relaxation may be worth investigation, it is clear that in order to use the RTIS technique to study isolated events the train repetition rate period must be greater than the t_R period of an iteration.

On the other hand, if the relaxation process takes significantly longer than 20 milliseconds the events will not be able to be repeated fast enough to appear as a still image to an observer. At this lower limit synchronization of the imaging laser pulse with a CCD camera is essential to properly record every frame. At much higher repetition rates, however, enough frames are produced that asynchronousity with the CCD camera is not an issue. A better statistical average is also obtained for higher repetition rates. For these reasons optimal results will be achieved when events are repeated as rapidly as possible while still allowing full (or near full) relaxation.

Spark Channel Relaxation

In order for the phenomenon of electric discharge induced breakdown to be suitable for RTIS imaging its relaxation period must be comparable to or less than 20ms. Since we are imaging breakdown with the thermal sensitive Schlieren method not only must the dielectric strength of the air fully relax but the spark channel's temperature must

also be allowed to relax back to the ambient value.

A simple but quite accurate model of spark channel decay has been developed by Schneider [24]. Both empirical evidence and his calculations indicate that for a 1 cm spark gap in air at STP dielectric strength will return to over 80% of its normal value within 10 ms of the spark's termination and will have virtually fully recovered by 100 ms. Similar levels of relaxation to ambient values are found for the average channel temperature at those times. This puts the maximum rep-rate range for a triggered spark at 100Hz to 10Hz, which just falls at the limit of RTIS applicability.

3 Experimental Apparatus

3.1 Ultrafast Laser Schlieren System

In Section 2.1 it was found that optimal Schlieren contrast can be obtained by maximizing the focal length of the focusing mirror, minimizing focal point size, and using longer wavelength light. In the table-top environment there was a strict constraint on the maximum focal length and mirror size due to space availability. This resulted in the choice of a 4.5” f-8 (focal length ~1 m) astronomical mirror for the piece “M” in Fig. 7, which allowed the fitting of the system on a table top. The laser used for the Schlieren apparatus was a Ti:Sapphire type lasing at 800 nm in the near IR region. This wavelength is ideal for quality Schlieren measurements because of the Gladstone-Dale coefficient's positive reliance on wavelength in Eq. 1 and the fact that near IR is still

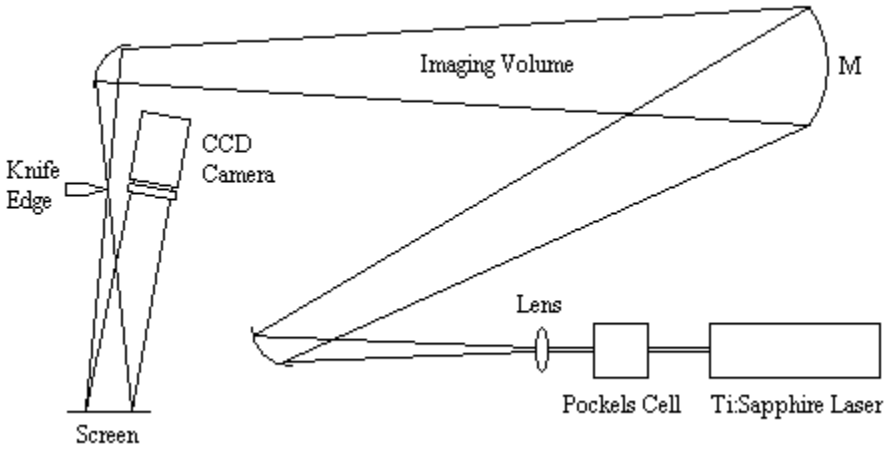

Fig. 7: Diagram of the ultrafast laser Schlieren system used in this study. The Pockels cell regulates a pulse train from the Ti:Sapphire laser in synchronization with triggered sparks within the volume.

within the limits of perception of CCD cameras. The mode-locked Ti:Sapphire generated a train of 50 femtosecond pulses which were culled by a triggered Pockels cell to produce a train of imaging pulses synchronized with the triggered sparks at a controllable rate.

3.2 Triggered Spark Generator

The design of the spark generator was guided primarily by the need for rapid generation of similar sparks and very low trigger jitter. An automotive ignition coil was selected to fulfill the first requirement due to its ability to deliver sparks of consistent quality reliably at speeds up to the kilohertz range. The coil was controlled by an IRF640N fast switching power MOSFET and TC4424 high load capability MOSFET driver to maximize the switching slew rate in accordance with Eq. 8. Also, the control circuitry and ignition coil were given separate power supplies with linear regulators and filter capacitors according to the manufacturers' recommendations to minimize voltage

ripple and noise. A schematic of the circuit without the ignition coil is shown in Fig. 8.

To ensure the MOSFET was completely switched on by the MOSFET driver a reference voltage of 7V was chosen for the control circuitry power supply. A resistor was placed between the driver and switch in order to damp out ringing from the MOSFET's gate capacitance. This resistance was made variable because the magnitude of the ringing could not be known beforehand and overdamping could be detrimental to the slew rate of the MOSFET driver.

To supply enough current for the ignition coil to generate a spark two high current LM338 regulators were tied in parallel as per the design idea put forth by Cavdar [25]. The voltage of this power supply was chosen to be 18V as a trade-off between maximizing the current drawn and staying within the specifications of the regulators and

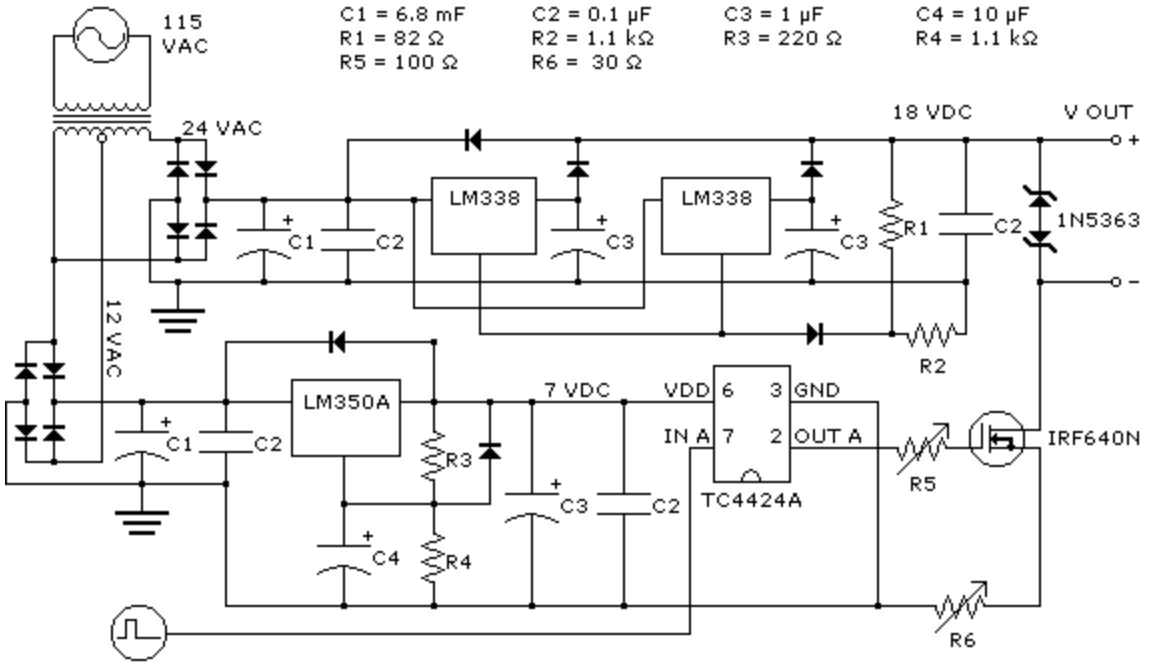

Fig. 8: Schematic of the low jitter spark generator used in this study, consisting of very stable power supplies and high slew-rate semiconductor switches to drive a spark coil attached to the output.

Fig. 9: Photograph of completed triggerable spark generator on prototype board with controls and spark coil.

mains transformer. In addition a 50W rheostat R6 was placed on the MOSFET's drain as a current limiter for the coil. Finally, two back-to-back 30 V breakdown Zener diodes were placed in parallel with the output to the coil in order to protect the circuit from high voltage inductive kickback. A photograph of the completed circuit beside the ignition coil and an improvised control housing is shown in Fig. 9.

4 Results

4.1 Schlieren System

The Schlieren system was successfully operated with both the pulsed IR Ti:Sapphire laser and a continuous green laser as a light source. The latter was used as a simple and easy source with which to test the basic Schlieren apparatus with visible light. Some images taken with the green laser are shown in Figs. 10 and 11. Two example images taken with the Ti:Sapphire are shown in Fig. 12. The concentric rings in these

images are thought to be caused by dust on the optics used. In order to obtain still shots of reasonable illumination the Ti:Sapphire was operated with each imaging pulse being made up of a burst of ten 50 fs pulses spaced 10ns apart, effectively resulting in a 100ns exposure. Using the fully amplified output from the complete laser system does not require the multi-pulse arrangement, so illumination would achieved using single 50fs pulse exposures.

No quantitative measurements were made with the system, nor was an estimate

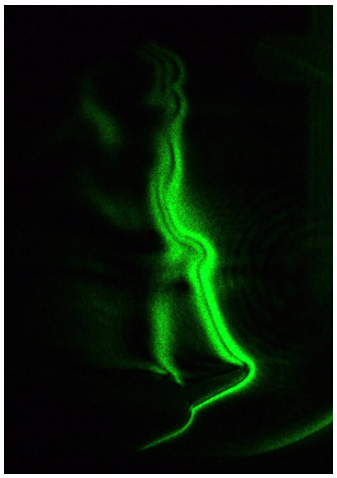

Fig. 10: Soldering iron Schlieren showing convection.

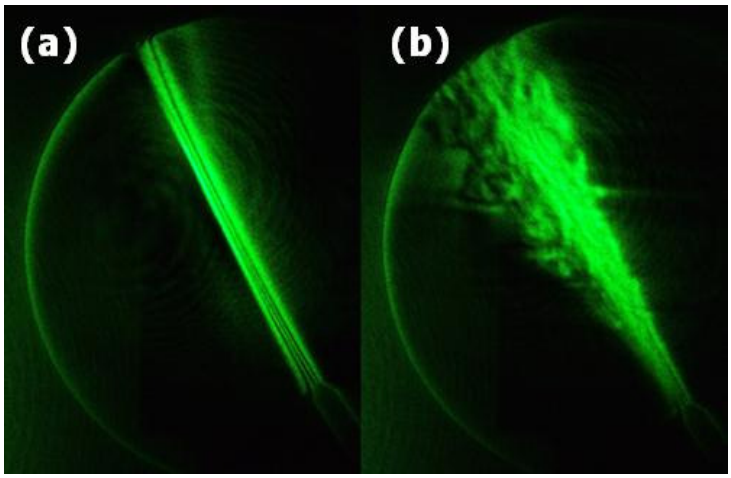

Fig. 11: Air jet Schlieren demonstrating laminar (a) and turbulent (b) flow.

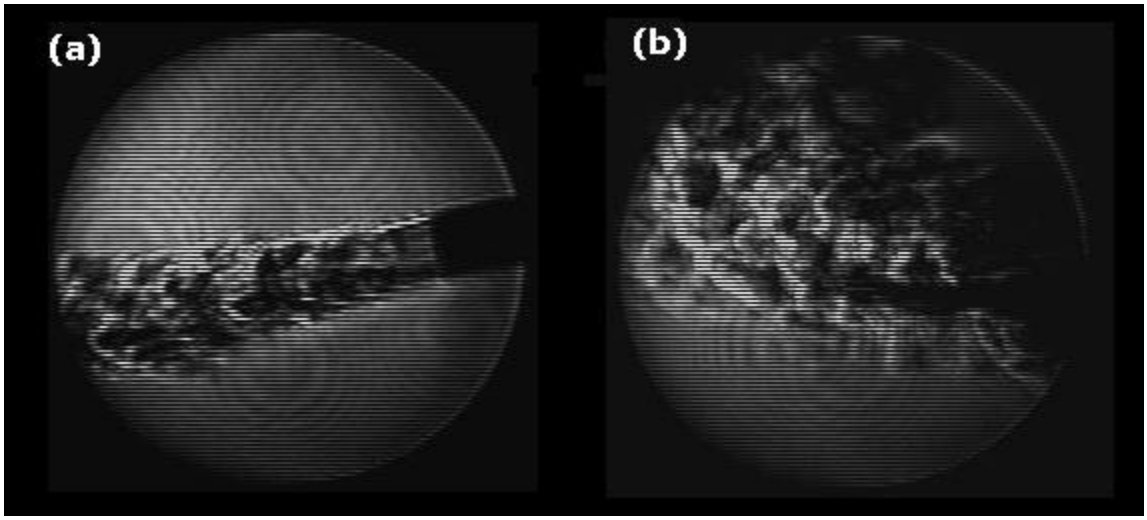

Fig. 12: Images with a relatively long 100ns exposure generated by the Ti:Sapphire laser: (a) turbulent airflow from an aerosol can and (b) airflow over a hot soldering iron tip.

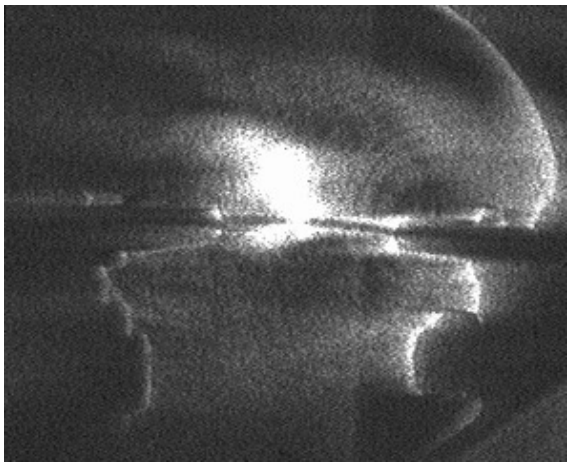

Fig. 13: CCD image exposed with the green laser of a spark gap firing at 60Hz. A large thermal plume is observed.

made of spatial resolution, though it is clearly <<1mm. Undesirable diffraction was a component in early images, but was able to be dramatically reduced with careful placement of imaging optics. When a spark was imaged with the green laser or at high rep-rate with the Ti:Sapphire a large thermal plume was observed (Fig.13).

4.2 Spark Generator

Some deviation was found between the designed power supply output voltages and their measured values, probably due to the tolerances of resistors R1-4. The actual values were within 1.15% of nominal for the driver and 16.3% for the coil (See Table 1) Both power supplies were found to be highly stable with maximum deviations of 0.022% and 0.013% respectively. There was no difference in these values between unloaded and loaded situations within the regulators' specifications. The MOSFET was found to have a critical gate voltage of 3.75 V, indicating that the driver was capable of providing sufficient voltage to completely turn it on.

Power Supply	Output (V)	Deviation (mV)	Associated Switch	Slew Rate (V/μs)	Jitter (ps)
Driver	6.85	±0.75	MOSFET Driver	130	11.5
Coil	15.08	±1.0	MOSFET	1400	1.43

Table 1: Spark generator voltage stability, slew rate, and temporal jitter data

The slew rates of the MOSFET driver and MOSFET were found by driving the circuit with a square wave from a Beckman Industrial FG2A function generator and measuring the falling edge slopes with a Tektronix 2235 oscilloscope. When plugged into Eq. 2.2.2 the measured values from the circuit yielded a jitter of 11.5 ps for the MOSFET driver and 1.4 ps for the MOSFET.

When the ignition coil was attached to the circuit's output it successfully produced triggered sparks across a point-point electrode gap when driven with a 7% duty cycle square wave at frequencies up to 5 kHz. However, the coil would not visibly discharge for an electrode gap larger than a few millimeters. This was found to be due to the ignition coil internally arcing over and thus limiting the length of any external spark. Occasionally it was observed that the falling edge of the trigger pulse would fall several nanoseconds after the proper time due to spurious triggering off of the spark instead of the function generator.

4.3 RTIS Imaging

The Schlieren system and spark generator were coupled via a Stanford Research

Systems DG353 digital delay generator and the spark gap electrodes' placed in the Schlieren imaging volume. This delay generator possesses a 50ps RMS specification jitter. It was found that the delay generator could directly drive the MOSFET without the MOSFET driver while maintaining high slew rate, thus eliminating 11.5ps of jitter from the system. Combined with an estimated Pockels cell jitter of 10-20ps and the remaining 1.4ps produced from the spark generator a working temporal resolution of 71ps was obtained. No method for synchronizing the CCD camera was employed, though this would have been desirable. Instead the RTIS system was driven at 100Hz and 10% duty cycle in order to produce enough frames to at least partially overcome asynchronousity with the camera while keeping the environment relaxation between sparks fairly complete. Frequencies up to 1kHz at 10% duty were examined, which is the limit for obtaining any significant relaxation between spark events.

It was found that the maximum spark length of the ignition coil was far too small for breakdown between the electrodes to be observed. Severe diffraction and generally blurry Schlieren images further exacerbated this inability to observe breakdown. No confirmable steady RTIS effects were observed in the thermal plume from the spark gap.

5 Discussion

The experiment successfully demonstrated that temporal resolution under 100ps is possible for semiconductor triggered spark gaps using the RTIS technique. This is comparable to the level of resolution offered by standard streak camera systems.

Occasional nanosecond jitter was observed in the spark generator due to spurious triggering off the spark, but this could be easily eliminated or at least greatly attenuated with a Faraday cage arrangement for the circuit.

The failure of the experiment to produce an RTIS image was due primarily to the inability of the ignition coil to produce a spark of sufficient length. A straightforward way to solve this problem would be to wind a custom transformer using high voltage wire. Though such a transformer is likely to be rather bulky due to the thick wire insulation there is no real impediment to its practicality. If the transformer were wound on a toroid of permeable material the emitted RF noise would be drastically reduced and perhaps aid in preventing unwanted secondary triggering of the circuit.

The other main reason the production of an RTIS image failed was insufficient spatial resolution of the Schlieren system. Diffraction from the knife edge is often the limiting factor in Schlieren spatial resolution, and many methods have been developed to highlight Schlieren without such a side effect. One of these, termed the phase knife-edge method, actually uses the diffraction to its advantage by interfering the Schlieren with each other by diffracting them through an Airy disk [26]. This method both eliminates diffraction from the final image and provides greater sensitivity than the solid knife-edge method. Spatial resolution be might further increased by focusing the laser beam down and passing it through a pinhole before expanding it onto the Schlieren mirror, thus providing a more point-like light source.

The final weakness of the RTIS system used here was its lack of synchronization between the CCD camera and the image pulse. Synchronization would have the benefit of

being able to drive the sparks at the lower frequency limit of RTIS and ensure complete environment relaxation between sparks while still capturing all image frames. Implementation would require triggering the camera from the delay generator via a PC interface and then effecting a synchronized image capture with software. The accomplishment of this feature is the keystone to more advanced RTIS techniques as it provides access to the real-time image processing capabilities afforded by modern computer technology.

6 Conclusion

An implementation of an RTIS system with subnanosecond temporal resolution for investigating electrical discharges in air has been demonstrated. While a successful example of RTIS imaging was not achieved, this was due to inadequacies in the system implementation and not the technique itself. Many improvements might be made to the basic system set forth here and it is believed that such revisions would allow the successful demonstration of a proof-of-principle experiment for RTIS. Other researchers are encouraged to adopt the RTIS method and explore its application in high-speed phenomenon that meet the candidacy criterion of reproducibility and relaxation.

Appendix A

To describe the deflection of a ray of light through a refractive index gradient we consider a coordinate system (Fig. A.1) such that the x-axis is parallel to the initial direction of light propagation and the y-axis runs parallel to a negative gradient $\Delta n/\Delta y$. This is essentially Fig. 2 rotated 90º clockwise and viewed in the x-y plane. As the ray travels a distance of Δx in the time Δt it is deflected an angle $\Delta\varepsilon$ as it passes through the gradient. The value of $\Delta\varepsilon$ may be found by considering the edges of the ray's wavefront located a distance Δy apart and propagating at two velocities due to the Δn difference in their local refractive indices, making one side Δc faster. Using the small angle approximation $\Delta\varepsilon \approx \tan(\Delta\varepsilon)$, the angle of refraction is:

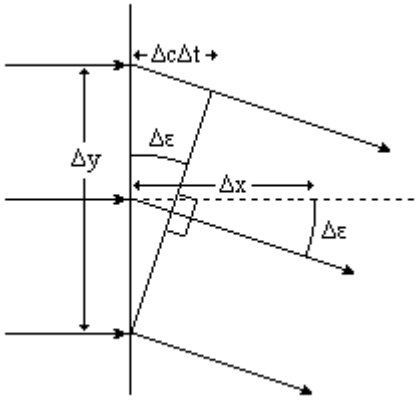

Fig. A.1: A wavefront of width Δy being diffracted by a gradient Δn/Δy through an angle Δε over a distance Δx.

$$\Delta\varepsilon = \frac{\Delta c\,\Delta t}{\Delta y} \tag{A.1}$$

And since the time differential Δt can be written as:

$$\Delta t = \frac{\Delta x}{c} \tag{A.2}$$

where c is the local speed of light for the ray, we may rewrite the angle of refraction as:

$$\Delta\varepsilon = \frac{\Delta c}{c}\frac{\Delta x}{\Delta y}$$

In order to convert from local light velocities to local indices of refraction we use the relation:

$$n = \frac{c_0}{c} \tag{A.3}$$

where the subscript 0 indicates vacuum, and expand $\Delta c/c$ as:

$$\frac{(c_2 - c_1)}{c} = \frac{(c_0/n_2 - c_0/n_1)}{c_0/n} = n\left(\frac{1}{n_2} - \frac{1}{n_1}\right) = \frac{n}{n_1 n_2}(n_2 - n_1)$$

Note that as Δy (and thus Δn) approaches zero the denominator $n_1 n_2$ approaches n^2, allowing us to write:

$$d\varepsilon = \frac{1}{n}\frac{dn}{dy}dx \tag{A.4}$$

Finally, accounting for a possible gradient along the z-axis and integrating we obtain:

$$\varepsilon_y = \int_o^L \frac{1}{n}\frac{\partial n}{\partial y}dx \tag{A.5}$$

with an analogous result for refraction in the z direction due to a $\partial n/\partial z$ gradient.

References

[1] **Control of filamentation induced by femtosecond laser pulses propagating in air**
Z. Jin, J. Zhang, M. H. Xu, X. Lu, Y. T. Li, Z. H. Wang, Z. Y. Wei, X. H. Yuan, and W. Yu, Optics Express 13,10424-10430 (2005)

[2] **Improved laser triggering and guiding of megavolt discharges with dual fs-ns pulses**
Guillaume Méjean, Roland Ackermann, Jérôme Kasparian, Estelle Salmon, Jin Yu, Jean-Pierre Wolf, Kay Rethmeier, Wilfried Kalkner, Philipp Rohwetter, Kamil Stelmaszczyk, and Ludger Wöste, Applied Physics Letters 88,021101 (2006)

[3] **Guided electric discharges induced by femtosecond laser filaments**
A. Ting, D.F. Gordon, D.F.; R.F. Hubbard, E. Briscoe, T. Jones, C. Manka, S.P. Slinker, A.P. Baronavski, H.D. Ladouceur, P.W. Grounds, P.G. Girardi, P. Speangle, 31st IEEE International Conference On Plasma Science (IEEE Cat. No.04CH37537), p. 262 (2004)

[4] **The variation with temperature of positive streamer properties in air**
N.L. Allen and A. Ghaffar, Journal of Physics D: Applied Physics Vol. 28 pp. 338-343 (1995)

[5] **Pulsed positive corona streamer propagation and branching**
E.M. van Veldhuizen and W. R. Rutgers, Journal of Physics D: Applied Physics Vol. 35, pp. 2169-2179 (2002)

[6] **Optical observation of prebreakdown phenomena in dielectric oil**
E. Morikawa, Electrical Engineering in Japan, Vol. 92, No. 1, pp. 11-17, (Jan.-Feb. 1972)

[7] **An ultra-high speed laser Schlieren technique for studying electrical breakdown in dielectric liquids**
W.R.L. Thomas, 1973 Annual Conference on Electrical Insulation and Dielectric Phenomena, pp. 130-136 (1974)

[8] **A comparison of negative and positive streamers in mineral oil at large gaps**
G. Massala and O. Lesaint, Journal of Physics D (Applied Physics), Vol. 34, No. 10, pp. 1525-32 (May 21, 2001)

[9] **Influence of molecular structure on propagation of positive streamer discharge dielectric liquid**
Y. Nakao, N. Hamano, T. Naito, Y. Nakagami, T. Shimizu, Y. Sakai, H. Tagashira Electrical Engineering in Japan, Vol. 149, No. 1, pp. 15-21, (Oct. 2004)

[10] **High-Speed Plasma Imaging: A Lightning Bolt**
G. A. Wurden and D. O. Whiteson, IEEE Trans. on Plasma Science, Vol 24, No. 1, pg 83-84. (Feb 1996)

[11] **Development of time resolved streak camera for the observation of lightning discharge**
X. Bounsou, I. Kitamura, K. Masugata, K. Kontani, Transactions of the Institute of Electrical Engineers of Japan, Part B, Vol. 126-B, No. 1, pp. 59-64 (2006)

[12] **Quantitative real-time pulsed Schlieren imaging of ultrasonic waves**
A. Hanafy, C.I. Zanelli, Ultrasonics Symposium, 1991. Proceedings., IEEE 1991, (1991)

[13] **Resolving the Sonoluminescence Pulse Shape with a Streak Camera**
R. Pecha, B. Gompf, G. Nick, Z. Q. Wang, and W. Eisenmenger
Physical Review Letters, Volume 81, Issue 3, pp.717-720 (Jul. 20, 1998)

[14] **Fast imaging of the plume expansion produced by laser ablation of LiNbO3**
A. Perea, J. Gonzalo, C.N. Afonso, C. Vivien, Ch. Leborgne
Applied Physics A: Materials Science & Processing, Volume 69, Number 7 (1999)

[15] **CCD sensor and camera for 100 Mfps burst frame rate image capture**
L. Lazovsky, D. Cismas, G. Allan, and D. Given
Proc. SPIE Vol. 5787, Airborne Intelligence, Surveillance, Reconnaissance (ISR) Systems and Applications II, Stephan H. Wyatt, Ed., pp. 184-190 (May 2005)

[16] **Photoelectronic techniques for subnanosecond evaluation of laser-material interactions and dynamic material properties**
D. L. Paisley, Proc. SPIE Vol. 1982, Photoelectronic Detection and Imaging: Technology and Applications '93, LiWei Zhou, Ed., p. 9 (Apr. 1993)

[17] **Temporal events in cyclopean vision**
T. J. Andrews, L. E. White, D. Binder, and D. Purves, Proc Natl Acad Sci USA. Vol. 93 No. 8, pp. 3689-3692 (Apr. 16 1996)

[18] **Beobachtungen nach einer neuen optischen Methode**
A. Toepler, Maximillan Cohen und Sohn, Bonn (1864)

[19] **On the use of laser light sources in schlieren-interferometer systems**
A. K. Oppenheim, P.A. Urtiew, and F.J. Weinberg
Proceedings of the Royal Society of London. Series A, Mathematical and Physical Sciences, Volume 291, Issue 1425, pp. 279-290 (1966)

[20] **Comment on explaining the mirage**
P. L. Dyson, American Journal of Physics, Volume 45, Issue 9, pp. 879-880 (Sept. 1977)

[21] **Schlieren and shadowgraph techniques: Visualizing phenomena in transport media**
G.S. Settles, New York: Springer (2001)

[22] **Electrical Breakdown of Gases**
J.M. Meek and J.D. Craggs, Chichester: Wiley (1978)

[23] **Electron drift velocity in hydrogen, nitrogen, oxygen, carbon monoxide, carbon dioxide and air at moderate E/N**
W. Roznerski and K. Leja, Journal of Physics D: App. Phys., Vol. 17, pp. 279-285 (1984)

[24] **Turbulent decay of after-spark channels**
M. N. Shneider, Physics of Plasmas, Volume 13, 073501 (2006)

[25] **High-current supply uses standard three-terminal regulator**
I. H. Cavdar, EDN, pp. 68-70 (Jul. 22, 2004)

[26] **Phase knife-edge laser Schlieren difraction interferometry with boundary difraction wave theory**
R. Kumar, D. Mohan, S.K. Kaurua, D.P. Chhachhia, and A.K. Aggarwal
Pramana Journal of Physics, Vol. 68, No. 4 (Apr. 2007)